MAGNETIC RESONANCE

Christoph Moenninghoff
Stefan Maderwald
Jens M. Theysohn
Oliver Kraff
Mark E. Ladd
Nicolai El Hindy
Johannes van de Nes
Michael Forsting
Isabel Wanke

Imaging of adult astrocytic brain tumours with 7 T MRI: preliminary results

C. Moenninghoff (✉) · S. Maderwald ·
J. M. Theysohn · O. Kraff ·
M. E. Ladd · M. Forsting · I. Wanke
Department of Diagnostic and
Interventional Radiology and
Neuroradiology,
University Hospital Essen,
Hufelandstraße 55,
45147 Essen, Germany
e-mail: christoph.moenninghoff@uk-essen.de
Tel.: +49-201-72384549
Fax: +49-201-7231563

C. Moenninghoff · S. Maderwald ·
J. M. Theysohn · O. Kraff ·
M. E. Ladd · M. Forsting · I. Wanke
Erwin L. Hahn Institute for Magnetic
Resonance Imaging,
University Duisburg-Essen,
Essen, Germany

N. El Hindy
Department of Neurosurgery,
University Hospital Essen,
Essen, Germany

J. van de Nes
Department of Neuropathology,
University Hospital Essen,
Essen, Germany

Abstract *Purpose:* In this study tumour vascularity and necrosis of intracranial astrocytomas were compared using 7 T and 1.5 T magnetic resonance imaging (MRI).
Methods: Fifteen patients with histologically proven astrocytomas (WHO grades II–IV) were prospectively examined at 1.5 T (Magnetom Espree or Sonata) and 7 T (Magnetom 7 T, Siemens, Erlangen, Germany) with T2*-w (weighted), T1-w with (only a subset of five patients at 7 T) and without contrast medium, T2-w and proton-density (PD)-w MRI. Clinically used 1.5 T sequences were adapted to 7 T. Histological findings and T2*-w MR images at both field strengths were compared for the presence of assumed tumour micro-vascularity and necrosis. Two diffusely infiltrating astrocytomas, four anaplastic astrocytomas and nine glioblastomas were included.
Results: T2*-w images depicted susceptibility patterns representing presumed tumour microvascularity in 8 out of 15 (53%) gliomas at 7 T compared with 5 out of 15 (33%) gliomas at 1.5 T. Compared with 1.5 T MRI three additional necrotic tumour areas were depicted only on 7 T T2- and T2*-w images of one glioblastoma. On T1-w MR images, contrast enhancement of five out of five glioblastomas was similar at both field strengths. *Conclusion:* 7 T gradient-echo sequences provide excellent image contrast of presumed microvasculature and necrosis in astrocytomas.

Keywords 7 Tesla · Astrocytoma · Microvascularity · Ultrahigh-field · MRI

Introduction

Since its clinical introduction in the 1980s, the magnetic field of magnetic resonance imaging (MRI) systems has increased gradually from low (0.1–0.5 T), through mid (0.5–1.5 T), to high fields (3 T) during the early 1990s and 2000s [1]. With the increased magnetic field, the signal-to-noise ratio (SNR) rises in an almost linear fashion and can be used to improve image quality especially in the field of neuroimaging. Ultrahigh-field MRI allows improved spatial resolution without sacrificing SNR and contrast-to-noise ratio (CNR) compared with low-field MRI [1]. Ultrahigh-field MR whole-body scanners for humans are currently available at 7 to 9.4 T.

Although MRI is the most sensitive imaging technique for detecting and assessing astrocytic brain tumours non-invasively [2], tumour type, grade and extent can only be determined with limited sensitivity and specificity by this imaging technique [3]. As demonstrated in first pilot studies, ultrahigh-field MRI ($B_0 \geq 7$ T) can provide high-

resolution images of brain tumours that cannot be achieved with the current lower-field-strength MR systems for clinical use [4, 5]. For neuroimaging the higher achievable SNR and increased sensitivity to susceptibility contrast are the important benefits of ultrahigh-field MRI.

Astrocytic brain tumours are the most frequent primary neoplasms of the central nervous system in adults, accounting for nearly 50% of all brain tumours [6, 7]. Diagnosis, therapy and prognosis almost exclusively depend on histopathological evaluation. The World Health Organisation (WHO) therefore provides the most common classification of astrocytomas based on their principal cell type, nuclear atypia, mitotic activity, microvascular proliferation and necrosis [6, 8].

In general, T2*-weighted gradient-echo sequences provide excellent image contrast of presumed microvasculature and microarchitecture in astrocytomas. Non-invasive visualisation of microvascularity appears to be one favourable clinical indication for brain tumour examinations at 7 T with possible benefits for glioma grading.

Diffusely infiltrating astrocytomas (WHO grade II) consist of well-differentiated gemistocytic or fibrillary neoplastic astrocytes with little cellularity, without mitotic activity and with minimal pleomorphic changes. On the other hand, anaplastic astrocytomas (WHO grade III) are characterised by increased mitotic activity, marked cellularity, and nuclear atypia, whereas necrosis or extended microvascularity are absent. Besides manifestation as a primary glioblastoma multiforme (GBM, WHO grade IV), astrocytic brain tumours WHO grades II and III can pass through malignant transformation to secondary GBMs [9]. Microvascular proliferation and/or necrosis, augmented mitotic activity of poorly differentiated astrocytic cells, a cellular and nuclear pleomorphism, and mostly central areas of necrosis are the histological hallmarks of glioblastomas.

The increased SNR and high susceptibility sensitivity of ultrahigh-field MRI provide the capability and opportunity to depict brain structures and tumour microvasculature within the submillimetre range, e.g. vessels of less than 100 μm in size [1, 5]. The sensitivity for susceptibility contrast increases with the applied magnetic field and allows the direct visualisation of microvasculature and blood products (e.g. deoxyhaemoglobin) within glioblastomas that cannot be achieved by low-field MR systems [4]. Sequence parameters optimised for MRI at 1.5 T or 3 T cannot be directly transferred to 7 T without major modifications to obtain optimal image quality. Increased image artefacts, e.g. chemical shift or susceptibility artefacts, specific absorption rate (SAR) limitations, and different tissue relaxation times force adaption of sequence parameters. At present, gradient- and spin-echo with T1, T2, T2* and PD weighting are the most commonly performed pulse sequences for brain imaging on ultrahigh-field MR systems. In this study, we sought to capture the different MR appearances of astrocytic brain tumours (WHO grades II–IV) at 7 T in comparison with 1.5 T MRI to demonstrate potential benefits of ultrahigh-field MRI in clinical applications.

Materials and methods

Patients

Over a period of 13 months, a total of 15 patients with suspected astrocytic brain tumours were prospectively enrolled from the department of neurosurgery at our institution. Only adult patients with untreated, presumably astrocytic brain tumours were examined with 1.5 T and 7 T MRI before neurosurgical operation. Merely patients presenting in good physical condition (Karnofsky scale ≥ 70) were eligible for the MR study. Before the MR examinations, informed written consent was obtained from each patient. The study was approved by the local ethics committee. MRI scans at 1.5 T and 7 T were both performed before needle biopsy or tumour resection and further therapy. Only patients with histological diagnosis of astrocytic brain tumours WHO grades II to IV were included in our study group, which consisted of six men and nine women aged from 30 to 69 years (mean age 53.9 years).

MR imaging techniques

For availability reasons, 1.5 T MR examinations were achieved with one of two conventional 1.5 T whole-body MR systems (Magnetom 1.5 T Espree or Sonata, Siemens Healthcare, Erlangen, Germany) equipped with a 12-channel, receive-only matrix head coil or a circularly polarised (CP) head coil (Siemens Healthcare, Erlangen, Germany), respectively. The 1.5 T MR examinations were acquired with a CP coil in seven patients and with a 12-channel head coil in eight patients. Ultrahigh-field MR examinations were performed on a 7 T whole-body MR system (Magnetom 7 T, Siemens Healthcare, Erlangen, Germany). Image acquisition in this study was performed with two different radiofrequency (RF) transmit/receive head coils: (1) a quadrature birdcage head coil (InVivo Diagnostic Imaging Corp., Gainesville, Florida, USA); and (2) an 8-channel head coil (Rapid Biomedical GmbH, Würzburg, Germany). For availability reasons 7 T MR examinations were performed with a CP coil in the first 3 patients and with an 8-channel head coil in the following 12 patients. Only in combination with the multi-channel head coil was the GRAPPA (generalized auto-calibrating partially parallel acquisition, acceleration factor of 2) reconstruction algorithm used to shorten total acquisition time of the 7 T multiplanar rapid acquisition gradient-echo

(MPRAGE) sequence in order to guarantee patient comfort and to limit motion artefacts. Partial Fourier imaging was applied in two dimensions with a factor of 6/8 to speed up image acquisition at both field strengths. The higher SNR at 7 T was exploited to achieve a smaller voxel size than at 1.5 T (Table 1).

Two- and three-dimensional spin-echo (SE) and gradient-echo (GRE) sequences were performed to obtain T2, proton-density-weighted (PD), MPRAGE and gradient-echo T2*-w MR images at 1.5 T and 7 T. A set of clinical MR sequences commonly used at 1.5 T were adapted to derive these sequences at 7 T. All sequences of the 7 T measurement protocol were initially optimised in healthy volunteers. The sequences were adapted to obtain optimal image contrast, complete coverage of the brain tumour and a higher spatial resolution within a reasonable examination time (Table 1). The time elapsed between the two MR examinations ranged from 0 to 14 days (mean interval 3.5 days). After phantom studies and testing in two healthy volunteers, gadolinium-enhanced T1-w images were obtained at 7 T after injection of a single dose (0.1 mmol/kg body weight) of gadopentetate dimeglumine (Magnevist®, Bayer Schering Pharma, Berlin, Germany) in 5 out of 15 patients. Total acquisition time at 1.5 T was approximately 25 min. As the double-echo spin-echo sequence needed several measurements for complete coverage of most tumours, total acquisition time at 7 T was approximately 45 min after individual shimming.

Image interpretation

The tumours were reviewed on 1.5 T and 7 T T2* images for foci of extensive or tortuous susceptibility patterns in the tumoral bed, presumably representing tumour microvascularity. The number of vessels in the tumoral bed was estimated relative to white matter penetrating vessels. It was graded as high if the density was greater than that of white matter, medium if the density was equal to that of white matter and low if it was less than that of white matter. This semiquantitative assessment of microvascular density on 1.5 T and 7 T gradient-echo images was compared with histopathological findings. The presence of microvascularity within the tumour mass was compared on T2*-w images and the presence of tumour necrosis was evaluated on 1.5 T and 7 T T2-w images.

Histology

Histological diagnosis was obtained for each tumour after MRI and neurosurgical operation by the department of neuropathology at our institution. The tumours were graded according to the WHO classification [9]. In ten patients stereotactic needle biopsy was guided to easily accessible tumour areas to guarantee patient safety. Surgical tumour resection was performed in five patients. Hence, large histological tumour sections were only available for five patients. The histology reports of all 15 patients and the histological sections of the 5 patients with macroscopic

Table 1 Imaging parameters for three MRI sequences acquired with 1.5 T and 7 T whole-body systems

Parameter	1.5 T MPRAGE ± contrast media	7 T MPRAGE ± contrast media	1.5 T PD/(T2)	7 T PD/(T2)	1.5 T T2*	7 T T2*
TR (ms)	2020	2500	3770	6000	721	750
TE (ms)	3.93	1.79	13 (81)	11 (95)	26	20.4
TI (ms)	1,100	1,100	–	–	–	–
FA (°)	15	6	150	150	20	59
Bandwidth (Hz/pixel)	130	570	130	257	78	30
FOV (mm^2)	230×230	256×208	230×173	256×256	230×187	256×173
Acquisition matrix (pixel)	512×256	512×353	256×192	512×512	256×156	512×384
Acquired voxel volume (mm^3)	0.4/0.9/1.25	0.5/0.6/0.8	0.9/0.9/5.0	0.5/0.5/3.0	0.9/1.2/6.0	0.5/0.5/3.0
Interpolated voxel volume (mm^3)	0.4/0.9/1.0	0.25/0.3/0.6	0.45/0.45/5.0	0.25/0.25/3.0	0.45/0.6/6.0	0.25/0.25/3.0
Slices	160	240	26	5	21	18
Parallel acquisition (acceleration factor)	No	GRAPPA (R = 2)	No	No	No	No
Acquisition time (min:s)	8:39	7:25	4:59	10:24	1:54	2:43

TR repetition time, *TE* echo time, *TI* inversion time, *FA* flip angle, *FOV* field of view

tumour resections were reviewed for the presence or absence of tumour vascularity.

Results

In this intraindividual study we compared presurgical 1.5 T and 7 T head MR images of 15 patients with histology-proven, diffusely infiltrating astrocytoma (WHO grade II, $n=2$), anaplastic astrocytoma (WHO grade III, $n=4$) and GBM (WHO grade IV, $n=9$). Among the 15 patients studied, a total of 15 masses were depicted at both field strengths. All lesions were supratentorially localised (Table 2). Four out of 15 lesions involved the corpus callosum. Tumour size ranged from 11 to 87 mm in axial diameter, mean diameter was 46.7 mm.

Reviewed histological reports confirmed atypical microvascularity in 6 out of 15 (40%) astrocytomas. Irregularly shaped vessel structures were visible in 8 out of 15 (53%) astrocytic tumours on 7 T T2*-w images and in 5 out of 15 (33%) astrocytic tumours on 1.5 T T2*-w images (Table 2). The semiquantitative analysis of vessel density in the tumour area resulted in a higher categorisation in all eight patients at 7 T compared with 1.5 T. Assumed pathological microvascularity was present on 7 T T2*-w images in four cases and on 1.5 T T2*-w images in two cases, contrary to the histological reports; on the other hand, microvascularity and/or endothelial hyperplasia was identified in the histological specimens in two cases, which was detected neither by 7 T nor 1.5 T MRI. On gadolinium-enhanced T1-w images, ring-shaped or heterogeneous contrast enhancement was noticed in ten high-grade gliomas (grade III, $n=1$; grade IV, $n=9$) at 1.5 T. Gadolinium-enhanced 7 T T1-w images were available in five patients (patients 6, 8, 12, 14, 15) with histologically proven high-grade gliomas (grade III, $n=1$; grade IV, $n=4$), displaying a similar contrast enhancement to 1.5 T T1-w images. The contrast between the ring-shaped, enhancing tumour mass and the central necrosis as well as the contrast between grey and white matter was reduced in 1.5 T T1-w images (Fig. 1a) compared with 7 T T1-w images (Fig. 1b). One hallmark of GBMs—tumour necroses—presented as hyperintense areas on T2- and T2*-w images of nine GBMs at both field strengths. Because of the small patient number and different histological tumour grades we present characteristic imaging findings in three illustrative cases.

Case no. 1

Figure 2 shows T2*-w GRE images of a diffusely infiltrating astrocytoma (WHO grade II) in the right parieto-occipital lobe of a 60-year-old female patient, who suffered from headache, dizziness, gait disturbance and focal motor seizures. MRI at 1.5 T revealed a non-enhancing tumour mass infiltrating the corpus callosum and displacing the occipital horn of the lateral ventricle (Fig. 2a). In addition to these macroscopic changes, only 7 T T2*-w GRE images displayed straight, transmedullary

Table 2 Demography, localisation, histological grading, and tumour microvascularity in 15 astrocytic brain tumours

Patient no.	Age (years)	Gender	Localisation	Grading (WHO)	Microvascularity at 7 T GRE	Microvascularity at 1.5 T GRE	Microvascularity in histology report	Histology sampling
1	33	F	Temporal	III	None	None	None	Biopsy
2	65	M	Frontal	IV	Low	None	EH, AM	Resection
3	59	F	Temporal	III	Medium	None	None	Biopsy
4	69	M	Temporal	IV	None	None	None	Resection
5	31	F	Temporal	III	Medium	Low	None	Biopsy
6	47	F	Frontal	IV	High	Medium	None	Biopsy
7	60	F	Temporoparietal	II	Low	None	None	Biopsy
8	52	M	Temporoparietal	IV	High	Medium	EH, AM	Biopsy
9	58	F	Frontal	II	None	None	None	Biopsy
10	30	F	Parietal	III	None	None	EH, AM	Biopsy
11	69	F	Frontoparietal	IV	Medium	Low	EH	Biopsy
12	61	M	Thalamic	IV	None	None	None	Biopsy
13	66	M	Parietal	IV	None	None	None	Resection
14	52	M	Temporo-occip-ital	IV	None	None	EH	Resection
15	57	F	Temporal	IV	High	Medium	EH	Resection

EH endothelial hyperplasia, *AM* atypical microvascularity, *M* male, *F* female

Fig. 1 Comparison of sagittal, contrast-enhanced T1-weighted images of a glioblastoma in the left temporal lobe. The irregular ring-shaped contrast enhancement of the high-grade glioma is comparable at both field strengths. However, the central necrosis, the signal intensity of intracranial vessels, and the contrast between grey and white matter is emphasised at 7 T (**b**). Compared with the 1.5 T image (**a**), the caudal coverage of the 7 T 8-channel head coil is reduced and motion artefacts around the eyeball are increased at 7 T
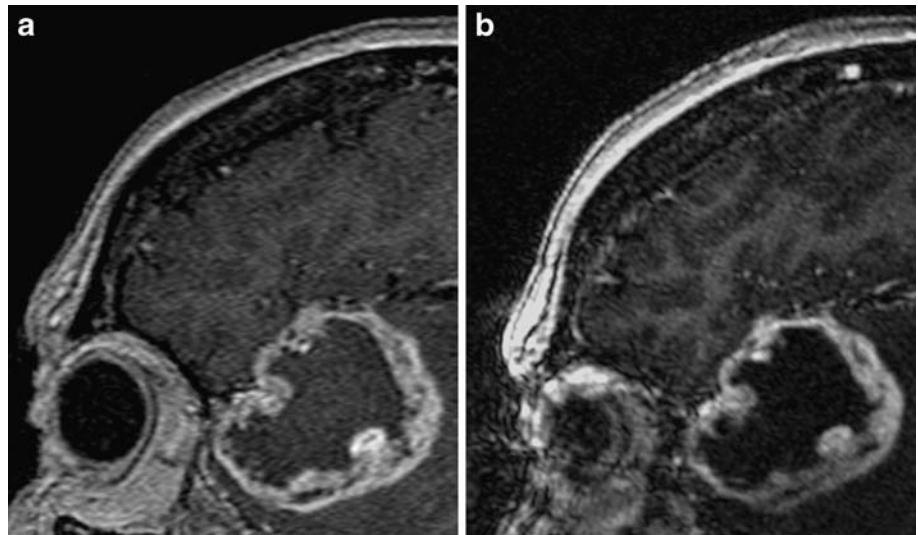
vessels in the hyperintense tumoral bed (Fig. 2b, black arrows) and surrounding brain regions. In the tumour area of the diffusely infiltrating astrocytoma (WHO grade II), only straight, penetrating vessels were identified in the white and grey matter. Tortuous and disorganised micro-vascularity and other characteristics of high-grade gliomas (contrast enhancement, cysts and oedema) were absent on 1.5 T and 7 T images.

Case no. 2

Figure 3 demonstrates T2*-w images of a 33-year-old female patient with left-sided hemiparesis caused by a tumour infiltrating the right basal ganglia and temporal lobe. The 7 T T2*-w images revealed an oval area of irregular signal intensity loss in the right putamen, which was surrounded by hyperintense tumour parts. The 1.5 T

T2*-w image (Fig. 3a) revealed heterogeneity of the tumour mass, but could not resolve the microarchitecture of this assumed focus of increased microvascularity as shown on the 7 T T2*-w image (Fig. 3b). This lesion was histologically graded as an anaplastic astrocytoma (WHO grade III) because of the absence of necrosis in all needle biopsies.

Case no. 3

A 47-year-old female patient presented with latent hemi-paresis of the right side of the body and increasing mental disorder. Contrast-enhanced 1.5 T T1-w images (not shown) revealed an annularly enhancing tumour mass of 7.4 cm in diameter localised in the left frontal lobe. At the time of diagnosis the brain tumour had already crossed the midline with invasion of the corpus callosum. After MRI,

Fig. 2 Comparison between 1.5 T (**a**) and 7 T (**b**) T2*-weighted GRE images of a diffusely infiltrating astrocytoma (WHO grade II) in the right parieto-occipital lobe crossing the midline through the splenium of the corpus callosum. The ultrahigh-field MR image depicts normal, transmedullary venous vessels (*black arrows*) in a straight course, which cannot be appreciated on the 1.5 T MR image. Because of the higher sensitivity for susceptibility contrast, calcifications and venous structures of the choroid plexus (*CP*) are larger and more hypointense at 7 T compared with 1.5 T
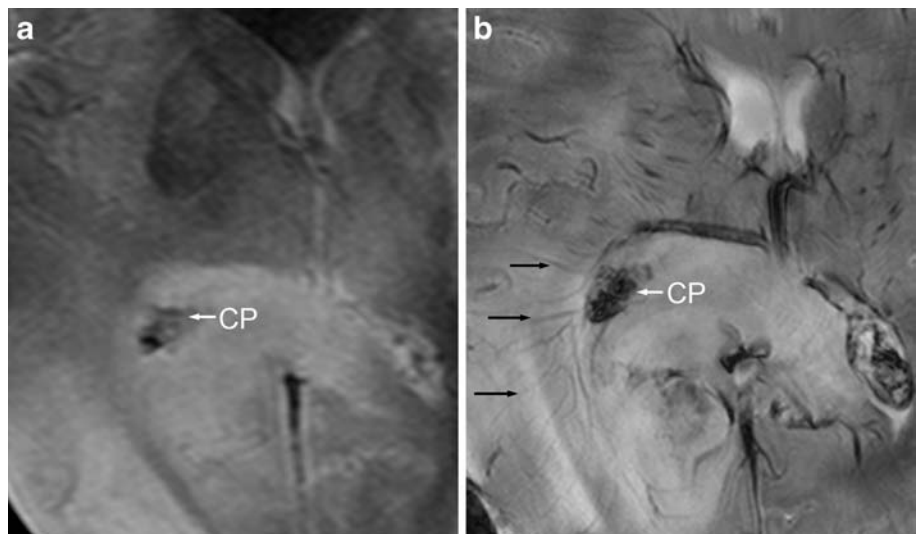
Fig. 3 T2*-weighted image (**b**) obtained on a 7 T MR system shows an oval area of irregular signal intensity loss in the centre of a biopsy-proven anaplastic astrocytoma in greater detail than the equivalent 1.5 T image (**a**). Because of their physiological iron content the basal ganglia are depicted as more hypointense on 7 T T2*-weighted images. *3V* third ventricle, *CND* caput of the caudate nucleus
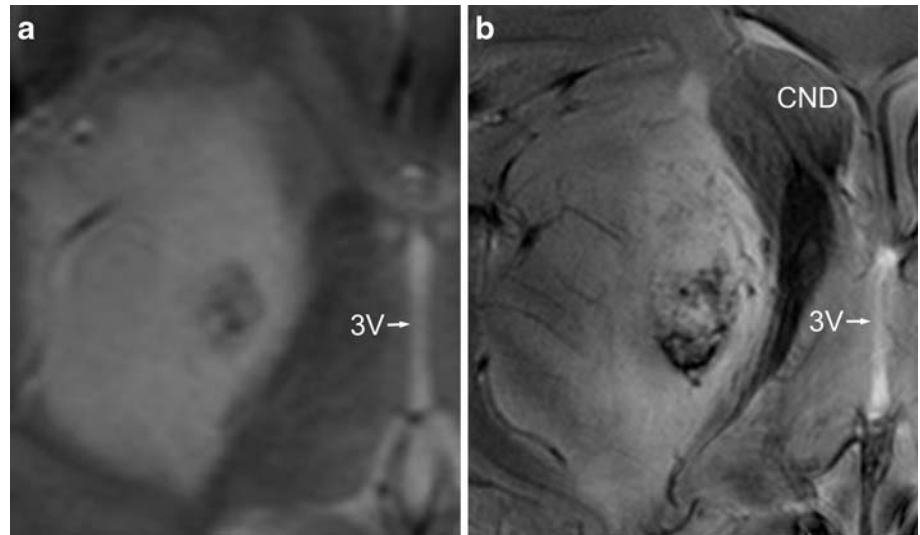
the patient was diagnosed with GBM (WHO grade IV) by needle biopsy. Histopathologically, the tumour was characterised by moderately increased cellularity, pleomorphic and hyperchromatic nuclei, and non-reactive necrosis. However, no atypical vasculature or endothelial proliferation was identified in the biopsy specimen. The 1.5 T T2-w images (Fig. 4a) revealed a large hyperintense area in the centre of the lesion, representing histologically confirmed necrosis. The corresponding 7 T T2-w image (Fig. 4b) provided a sharper delineation of the central necrosis and outlined three smaller necroses in the peripheral parts of the tumour bed. Irregular areas of signal intensity loss in the tumour area were best displayed on 7 T T2*-w images, presumably representing tumour microvascularity (Fig.5b). In addition to straight, transmedullary vessel structures in unchanged brain regions representing regular microvasculature, assumed tumour microvascularity consisted of irregularly shaped and tortuous vessels. The inherently lower resolution of the 1.5 T T2*-w image (Fig. 5a) only allowed the identification of the largest venous vessels in this area, whereas irregularly shaped microvasculature could be clearly identified on 7 T T2*-w images of the same tumour areas. Enlarged transmedullary vessels were found in the superior rim of the same glioblastoma, presumably representing draining veins from the tumoral bed (Fig. 6b).

Discussion

The higher achievable signal-to-noise ratio (SNR) and the increased sensitivity to susceptibility contrast are the main advantages of ultrahigh-field MR systems for clinical applications. The SNR increases with field strength in almost linear fashion, so that it is theoretically three- to fourfold higher at 7 T compared with 1.5 T [10–12]. With

Fig. 4 Hyperintense necrosis (*N*) in the centre of a glioblastoma multiforme. Because of the higher SNR and spatial resolution the axial T2-weighted spin-echo MR image at 7 T (**b**) reveals more and smaller necroses in the tumour bed (*arrows*) compared with the equivalent 1.5 T image (**a**), which was obtained by use of a clinical measurement protocol
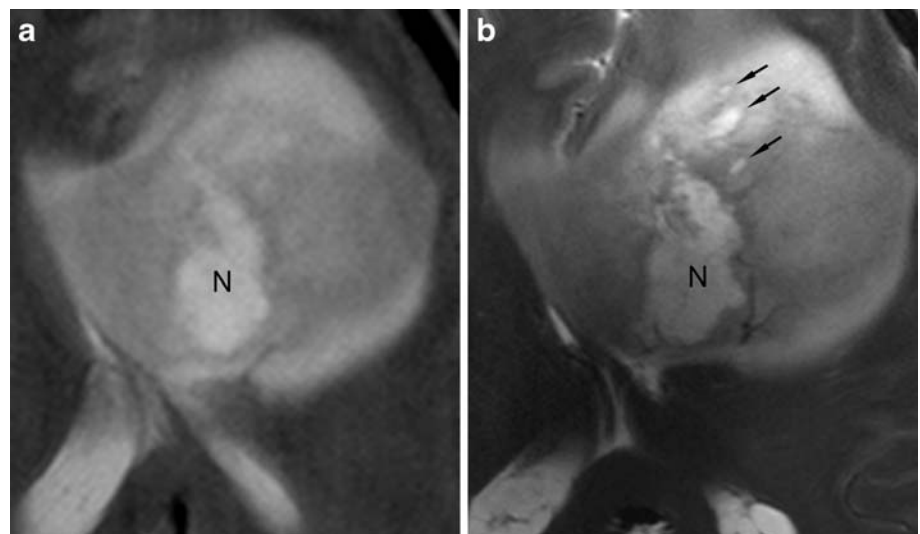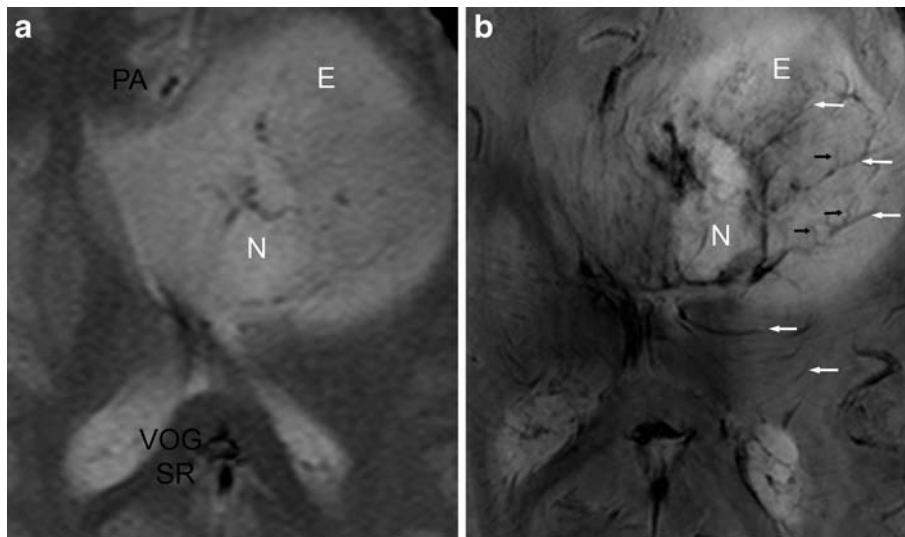
Fig. 5 Normal vasculature and presumed tumour vascularity in a glioblastoma in the left frontal lobe. Comparison is made between an axial T2*-weighted GRE image at 1.5 T (**a**, 256×192 matrix size) and the corresponding image at 7 T (**b**, 512×512 matrix size). The irregular, hypointense vessel structures in the tumour bed (*black arrows*) presumably represent tumour microvascularity. Straight transmedullary vessel structures in the tumour bed and in adjacent, physiological brain regions (*white arrows*) represent normal microvasculature. The 1.5 T MRI can only depict large vessel structures like the vena of Galen (*VOG*), the sinus rectus (*SR*) and the pericallosal artery (*PA*). *N* central necrosis, *E* perifocal oedema

increasing field strength, susceptibility contrast of paramagnetic substances (e.g. deoxyhaemoglobin) is amplified and allows a superior depiction of venous vasculature and microhaemorrhages [1, 13].

In astrocytic neoplasms, angiogenesis is one marker of tumour aggressiveness and a precondition of tumour growth [14, 15]. Tumour vessels are often more tortuous and disorganised than normal brain vessels. Among other criteria, histopathological grading of astrocytomas is based on the assessment of tumour vascularity, using endothelial cytology or staining techniques to quantify angiogenesis. In astrocytomas, microvascularity increases from low- to high-grade gliomas [9, 16]. In this study we classified the number of tumour vessels relative to the number of normal white matter penetrating vessels in three different categories (low, medium, high) on T2*-w images at 7 T and 1.5 T. Exploiting the increased sensitivity of susceptibility contrast and the higher achievable spatial resolution of 7 T MRI, we could not only find evidence for an increasing microvascularity from low- to high-grade gliomas, but also an improved depiction of tumour vascularisation at 7 T compared with 1.5 T (Table 2). Hence, the non-invasive depiction and monitoring of cerebral microvasculature may possibly be improved by 7 T MRI. Pilot studies of two patients with glioblastoma compared high-resolution gradient-echo 8 T MR images with cerebral angiography in

Fig. 6 Comparison of T2*-weighted MR images at 1.5 T (**a**) and 7 T (**b**) achieved at the superior border of a glioblastoma in the same patient. Dilated, transmedullary vessel structures (*arrows*) are thought to represent draining veins coursing over the tumour bed and connecting to cortical veins. The 7 T image (**b**) shows thin, straight signal voids (*arrowheads*) consistent with the normal angioarchitecture of the white matter
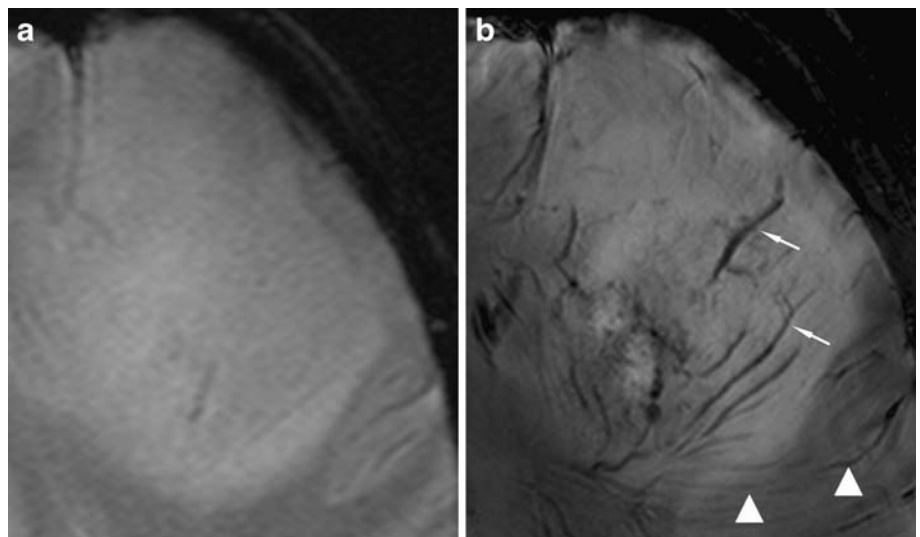
vivo and in an embalmed brain post mortem suggesting a good correlation of abnormal microvascularity within the tumours [4, 17]. Recently, the lenticulostriate arteries were visualised by 7 T MR angiography in vivo, and the depiction of microvasculature as small as 100 μm was achieved by ultrahigh-field MR systems [5, 18]. At 1.5 T and 3 T other important MR techniques for the evaluation of tissue vascularity like perfusion MRI and dynamic susceptibility contrast-enhanced MRI measure the increased cerebral blood flow and blood volume in tumour areas, but with limited morphological information compared with T2*-w images [19, 20]. Neither technique is currently established for 7 T MRI.

In this preliminary study we focused our image analysis on T2* information, because image information and susceptibility contrast of this sequence were very different compared with its 1.5 T equivalent. Hence, assumed tumour microvascularity was displayed more detailed on 7 T compared with 1.5 T T2*-w images. The 7 T and 1.5 T GRE images of 15 patients with histology-proven astrocytic brain tumours (WHO grades II–IV) were compared with the histopathological features of microvascularity to determine if assumed signal voids and vessel structures correlate with histopathological findings.

In agreement with previous studies at 7 T and 8 T, the venous vasculature was depicted with high contrast and great detail on T2*-w images [5, 11, 17, 21, 22]. In addition to small transmedullary vessels in normal brain regions of all subjects, 7 T T2*-w images demonstrated irregular tumour microvascularity in 8 out of 15 astrocytic brain tumours with more detail than corresponding 1.5 T T2*-w images. Compared with 1.5 T GRE sequences, signal voids attributable to venous vessels were markedly increased in 7 T GRE sequences, as venous blood has a short T2* time because of the magnetic susceptibility of deoxyhaemoglobin [23]. On the other hand, arterial blood is close to 100% saturated with oxygen. Its longer resulting

T2* time precluded emphasis of arterial vessels on the gradient-echo sequences used in this study. The higher achievable spatial resolution of 7 T T2*-w images with $0.5 \times 0.5 \times 3.0$ mm^3 voxel size allowed the detection of more and smaller microvasculature of the brain compared with equivalent 1.5 T T2*-w images with $1.2 \times 0.9 \times 6.0$ mm^3 voxel size.

Limitations of ultrahigh-field MR systems

At 7 T chemical shift between fat and water is about 1,000 Hz compared with 214 Hz at 1.5 T, resulting in emphasised image artefacts at 7 T. These artefacts can be reduced by increasing the receiver bandwidth [24]; however, this implies a reduction of SNR. As a result of the higher susceptibility sensitivity at 7 T, image quality of gradient-echo sequences may be reduced compared with at 1.5 T because of local magnetic field inhomogeneities near the skull base and the aerated paranasal sinuses. These artefacts could possibly prevent the depiction of brain tumours located in basal parts of the brain. In comparison with 1.5 T MRI, whole-brain imaging at 7 T is restricted by SAR limitations for most sequences. Changes in tissue relaxation times can lead to altered contrast behaviour at 7 T. Specific absorption rate limitations, different tissue relaxation times and more severe image artefacts of 7 T MRI definitely require adjustments of sequence parameters from those used at lower field strengths (Table 1).

Study limitations

In this study 1.5 T and 7 T MR imaging were compared, because a 3 T MRI system is not available in our institution. Although 3 T MRI may provide better image quality than 1.5 T MRI, the latter is still the most

Fig. 7 Haematoxylin–eosin (HE)-stained sections of a glioblastoma multiforme. **a** Histological specimen (HE stain, ×100) shows multiple vessels of varying size with endothelial hyperplasia and several atypical vessel proliferations in an area of high vascular density. **b** Another area of the same tumour (HE stain, ×200) reveals pleomorphic nuclei, mitoses and cellular atypia, but no pathological vessels are detected
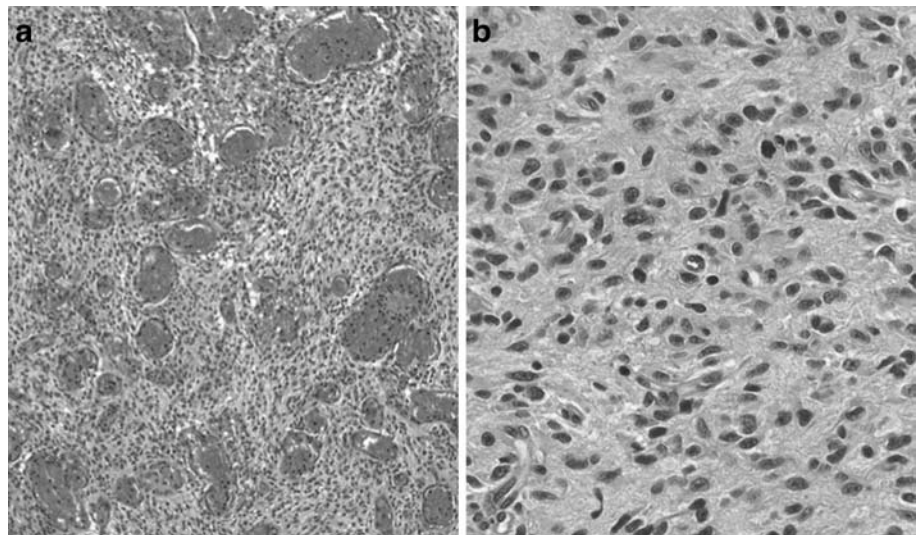
commonly utilised field strength in clinical applications and accessible to most radiologists.

As a result of SAR limitations, sequences with high energy deposition like double-echo TSE mandated several measurements at 7 T to obtain complete coverage of most brain tumours. This factor and the acquisition of thinner sections are the reasons for the nearly doubled acquisition time from 25 min for 1.5 T MRI to 45 min for 7 T MRI. One major limitation of this study is the fact that the location of tumour vascularity in histological tumour sections or biopsy specimens could not be directly linked to foci of tumour microvascularity on MR images. Routine needle biopsies were performed in ten patients to get tumour tissue for histological assessment (Fig. 7). For reasons of patient safety, biopsy needles were guided to easily accessible tumour areas. Hence, the sampling of tumour vessels and necrosis within the biopsy specimen was rather unsystematic. Because of the small sample size, needle biopsies can miss areas of pathological microvascularity. This fact may explain the identification of vascular disorders in eight patients on 7 T T2*-w images (Table 2) contrary to the "gold standard" of histopathology with atypical vascularity in six patients.

Although our study population only consisted of 15 patients with astrocytic brain tumours, this preliminary study suggests strong evidence that a potential application of 7 T GRE imaging is the depiction of tumour microvascularity in vivo. Low-grade gliomas tend to progress into high-grade gliomas with increasing vascular changes and abnormalities. Under conservative treatment, monitoring of low-grade gliomas and early detection of malignant transformation are essential to allow accurate prognostication and suitable treatment planning. Hence, 7 T MRI may develop as a valuable tool for assessment of tumour vascularity and for the monitoring of anti-angiogenic therapies of brain tumours.

In summary, 7 T MRI offers more detailed depiction of tumour microvascularity and necrosis within intracranial gliomas because of higher achievable spatial resolution and increased sensitivity for susceptibility contrast compared with 1.5 T MRI. This developing imaging technique may provide useful information for grading gliomas and for monitoring tumour angiogenesis and anti-angiogenetic therapies. Optimised multi-channel head coils, tailored imaging protocols and new parallel imaging techniques are expected to further improve image quality of ultrahigh-field MRI.

References

1. Yuh WT, Christoforidis GA, Koch RM et al (2006) Clinical magnetic resonance imaging of brain tumors at ultrahigh field: a state-of-the-art review. Top Magn Reson Imaging 17:53–61
2. Behin A, Hoang-Xuan K, Carpentier AF, Delattre JY (2003) Primary brain tumours in adults. Lancet 361:323–331
3. Croteau D, Scarpace L, Hearshen D et al (2001) Correlation between magnetic resonance spectroscopy imaging and image-guided biopsies: semiquantitative and qualitative histopathological analyses of patients with untreated glioma. Neurosurgery 49:823–829
4. Christoforidis GA, Grecula JC, Newton HB et al (2002) Visualization of microvascularity in glioblastoma multiforme with 8-T high-spatial-resolution MR imaging. AJNR Am J Neuroradiol 23:1553–1556
5. Dashner RA, Kangarlu A, Clark DL, RayChaudhury A, Chakeres DW (2004) Limits of 8-Tesla magnetic resonance imaging spatial resolution of the deoxygenated cerebral microvasculature. J Magn Reson Imaging 19:303–307
6. Silverberg E, Boring CC, Squires TS (1990) Cancer statistics, 1990. CA Cancer J Clin 40:9–26
7. Burger PC, Vogel FS, Green SB, Strike TA (1985) Glioblastoma multiforme and anaplastic astrocytoma. Pathologic criteria and prognostic implications. Cancer 56:1106–1111
8. Louis DN, Ohgaki H, Wiestler OD et al (2007) The 2007 WHO classification of tumours of the central nervous system. Acta Neuropath 114:97–109
9. Kleihues P, Louis DN, Scheithauer BW et al (2002) The WHO classification of tumors of the nervous system. J Neuropathol Exp Neurol 61:226–229
10. Abduljalil AM, Kangarlu A, Yu Y, Robitaille PM (1999) Macroscopic susceptibility in ultra high field MRI. II: acquisition of spin echo images from the human head. J Comput Assist Tomogr 23:842–844
11. Burgess RE, Yu Y, Christoforidis GA et al (1999) Human leptomeningeal and cortical vascular anatomy of the cerebral cortex at 8 Tesla. J Comput Assist Tomogr 23:850–856
12. Vaughan JT, Garwood M, Collins CM et al (2001) 7 T vs 4 T: RF power, homogeneity, and signal-to-noise comparison in head images. Magn Reson Med 46:24–30
13. Dashner RA, Chakeres DW et al (2003) MR imaging visualization of the cerebral microvasculature: a comparison of live and postmortem studies at 8 T. AJNR Am J Neuroradiol 24:1881–1884
14. Folkman J (1995) Angiogenesis in cancer, vascular, rheumatoid and other disease. Nat Med 1:27–31
15. Abramovitch R, Meir G, Neeman M (1995) Neovascularization induced growth of implanted C6 glioma multicellular spheroids: magnetic resonance microimaging. Cancer Res 55:1956–1962
16. Brem S, Cotran R, Folkman J (1972) Tumor angiogenesis: a quantitative method for histologic grading. J Natl Cancer Inst 48:347–356
17. Christoforidis GA, Kangarlu A, Abduljalil AM et al (2004) Susceptibility-based imaging of glioblastoma microvascularity at 8 T: correlation of MR imaging and postmortem pathology. AJNR Am J Neuroradiol 25:756–760
18. Cho ZH, Kang CK, Han JY et al (2008) Observation of the lenticulostriate arteries in the human brain in vivo using 7.0 T MR angiography. Stroke 39:1604–1606

19. Di Costanzo A, Pollice S, Trojsi F et al (2008) Role of perfusion-weighted imaging at 3 Tesla in the assessment of malignancy of cerebral gliomas. Radiol Med 113:134–143

20. Ulmer S, Liess C et al (2009) Use of dynamic susceptibility-contrast MRI (DSC-MRI) to assess perfusion changes in the ipsilateral brain parenchyma from glioblastoma. J Neurooncol 91:213–220

21. Christoforidis GA, Bourekas EC, Baujan M et al (1999) High resolution MRI of the deep brain vascular anatomy at 8 Tesla: susceptibility-based enhancement of the venous structures. J Comput Assist Tomogr 23:857–866

22. Ogawa S, Lee TM (1990) Magnetic resonance imaging of blood vessels at high fields: in vivo and in vitro measurements and image simulation. Magn Reson Med 16:9–18

23. Ogawa S, Lee TM, Kay AR, Tank DW (1990) Brain magnetic resonance imaging with contrast dependent on blood oxygenation. Proc Natl Acad Sci USA 87:9868–9872

24. Bernstein MA, Huston J 3rd, Ward HA (2006) Imaging artifacts at 3.0 T. J Magn Reson Imaging 24:735–746